JMEPEG (2016) 25:518–529
DOI: 10.1007/s11665-016-1891-0

1059-9495/$19.00

Electrochemical Corrosion Behavior of Thermal-Sprayed Stainless Steel-Coated Q235 Steel in Simulated Soil Solutions

Wei Wei, Xin-qiang Wu, Wei Ke, Song Xu, Bing Feng, and Bo-tao Hu

(Submitted May 24, 2015; in revised form December 8, 2015; published online January 14, 2016)

The corrosion behavior of a thermal-sprayed stainless steel (SS)-coated Q235 steel has been investigated in simulated soil solutions using electrochemical measurements, x-ray photoelectron spectroscopy analysis, and scanning electron microscope. The as-received Q235 steel and galvanized steel for grounding grids were also examined for the purpose of comparison. The effects of pH value of testing solutions have been examined. The thermal-sprayed SS-coated steel showed the best corrosion resistance among the three kinds of materials. With increasing pH value, the corrosion resistance of SS-coated Q235 steel increased. In weak alkaline solutions, the SS-coated Q235 steel showed the largest polarization resistance (3.2×10^5 Ω cm^2), the lowest anodic current density (1.4×10^{-2} μA/cm^2), and the largest film resistance (4.5×10^6 Ω cm^2), suggesting that the coated steel has the best corrosion resistance in weak alkaline environment. Related corrosion mechanisms are also discussed.

Keywords corrosion resistance, corrosion scales, electrochemical behavior, grounding grids, pH value, stainless steel, thermal spraying

1. Introduction

Substations grounding grids play an important role in maintaining the stable operation of power system and ensuring the safety of operators and equipment. China mainly uses ordinary carbon steels typically such as Q235 steel or galvanized steel (hot-dipped Zn-coated carbon steel) as grounding materials at present. But these two materials are prone to corrosion when they are buried in the complex soil environments (Ref 1-4). Some grounding grids suffer from severe corrosion and even break during long-term service, which directly threats to the security of power system. Because the area of the grounding grids is very large, and usually buried deeply under the ground, it is rather difficult and costly to on-site protect, overhaul, repair, or replace in-service undergrounding grids. Although copper materials or copper-coated steels have been used as common grounding materials in US, Japan, and many European countries (Ref 5, 6), these materials still have many deficiencies when used as grounding grids. In the first place, the copper grounding grids will accelerate the corrosion of adjacent steel frame. In the second place, copper is a strategic material in China, and the resource is not rich. Furthermore, the buried copper will cause serious pollution to the water and soil. Finally, copper has good corrosion resistance in alkaline soil, but in the acidic soil, its corrosion resistance is similar to iron. Therefore, there is no doubt that copper is not the ideal grounding material for China (Ref 7, 8). For the above reasons, it is necessary to understand the corrosion behavior and mechanism of the grounding materials and develop corresponding protective methods or on-line diagnosis techniques.

An ideal grounding material must have the following characteristics: Firstly, the grounding grids should have enough heat stability to sustain the powerful grounding current. Secondly, the grounding grids should have good corrosion resistance to meet the requirement of service life. Thirdly, the grounding materials should have rich resources and moderate cost. Moreover, the grounding materials should be easy to process and construct. Last but not the least, the grounding grid should not accelerate the corrosion of the adjacent steel frame.

In recent years, arc thermal spraying metal coatings have been widely applied to the engineering of the corrosion and machine protection (Ref 9-11). The metals used for spraying usually include zinc, aluminum, and stainless steels, etc. Generally, thermal spraying method is the use of compressed air to make the molten metal atomize into micro drops, and make them deposit on the prepared substrate surface at high speed to form a complete metal layer. According to the different corrosion environments, corresponding corrosion resistant coatings can be chosen, and the coating thickness can be easily controlled. Hot dip galvanized methods, by contrast, can only prepare zinc coating, and the thickness of the coating is very limited. The technique of thermal spraying is very simple and easy to operate. During the process of spraying, the temperature of the substrate surface is relatively low and can be controlled, thus it has little impact on the microstructure and mechanical properties of the substrate, and the deformation of the workpiece is also small. In addition, the technique of arc thermal spraying has low cost but high efficiency, which make

Wei Wei, Xin-qiang Wu, and **Wei Ke**, Key Laboratory of Nuclear Materials and Safety Assessment, Liaoning Key Laboratory for Safety and Assessment Technique of Nuclear Materials, Institute of Metal Research, Chinese Academy of Sciences, Shenyang 110016, People's Republic of China; and **Song Xu, Bing Feng,** and **Bo-tao Hu**, Hunan Electric Power Corporation Research Institute, Changsha 410007, People's Republic of China. Contact e-mail: xqwu@imr.ac.cn.

it become the preferred technology in spraying large area anti-corrosion engineering structures. The coating made by thermal spraying method has many advantages, such as compact, homogeneous, strong adhesion, and so on. Thus, in industrial atmosphere, seawater, and soil environments, the thermal spraying technique has greatly increased the service life of steel structures, which can reach more than 20 years (Ref 12).

In the present work, electrochemical corrosion behaviors of thermal-sprayed stainless steel (SS)-coated Q235 steel, as-received Q235 steel, and galvanized steel have been investigated in simulated soil solutions. Effects of pH values of solutions on the corrosion behavior of the above materials have been examined. Related corrosion mechanisms are also discussed.

2. Experimental

2.1 Experimental Material

The as-received Q235 steel sheet and galvanized steel sheet for grounding grids investigated in the present work were taken from Hunan Provincial Electric Power Corporation. The chemical compositions of the Q235 steel are 0.18C, 0.50Mn, ≤ 0.30Si, ≤ 0.050S, ≤ 0.045P, and Fe balance. The thickness of Zn coating for the galvanized steel is about 85 μm.

The SS coating consisting of 18 wt.% Cr, 9 wt.% Ni, 1 wt.% Ti, and Fe balance was prepared on the as-received Q235 steel sheet using an arc thermal spraying method. The Q235 steel sheet with dimensions of 80 × 80 × 5 mm was

Table 1 Simulated soil solutions used in this study

Solutions	pH Value	Na_2SO_4, mg/L	$NaHSO_4{\cdot}H_2O$, mg/L	$MgCl_2{\cdot}6H_2O$, mg/L	NaOH, mg/L
1	3.53	…	447.5	26.04	…
2	4.79	…	8.95	26.04	…
3	7.03	9.216	…	26.04	…
4	9.60	9.216	…	26.04	4
5	12.26	9.216	…	26.04	400

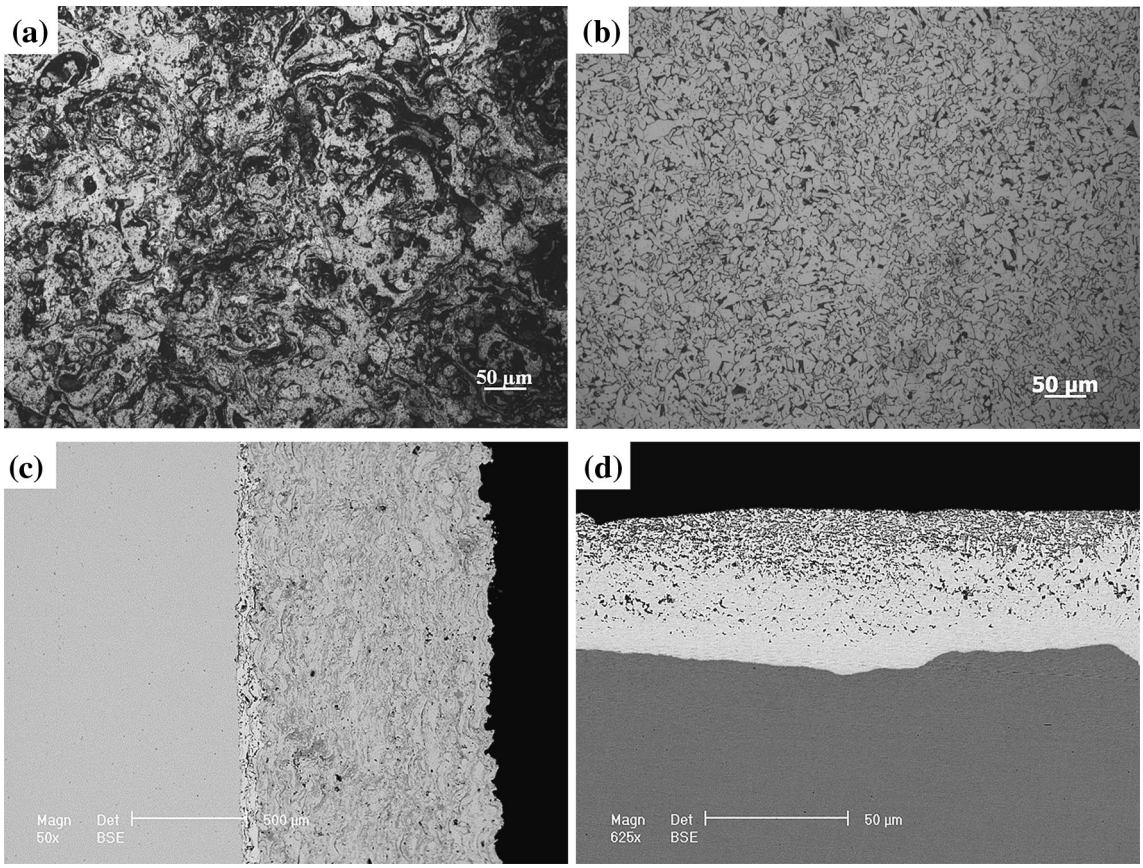

Fig. 1 Microstructures of the three steels used in the present work: (a) the surface morphology of thermal-sprayed SS-coated steel; (b) the surface morphology of as-received Q235 steel; (c) the cross-section microstructure of thermal-sprayed SS-coated steel; (d) the cross-section microstructure of galvanized steel

Table 2 Fitted polarization resistance (R_p) values (Ω cm^2)

pH value	Q235 steel	Galvanized steel	SS coating
3.53	483	971	1441
4.79	6575	8570	15230
7.03	9206	10862	247164
9.60	9227	8513	315370
12.26	180829	84399	299300

used as substrate. The substrates were degreased ultrasonically in acetone and grit blasted with corundum in order to remove any contamination from the surface and generate roughened surface that promotes coating adhesion. In order to get a better bonding between the substrate and coating, a Ni bond layer was sprayed between them. Compressed air was used to remove any residue from the grit blasting. The arc spraying voltage and current were 48 V and 120 to 130 A, respectively.

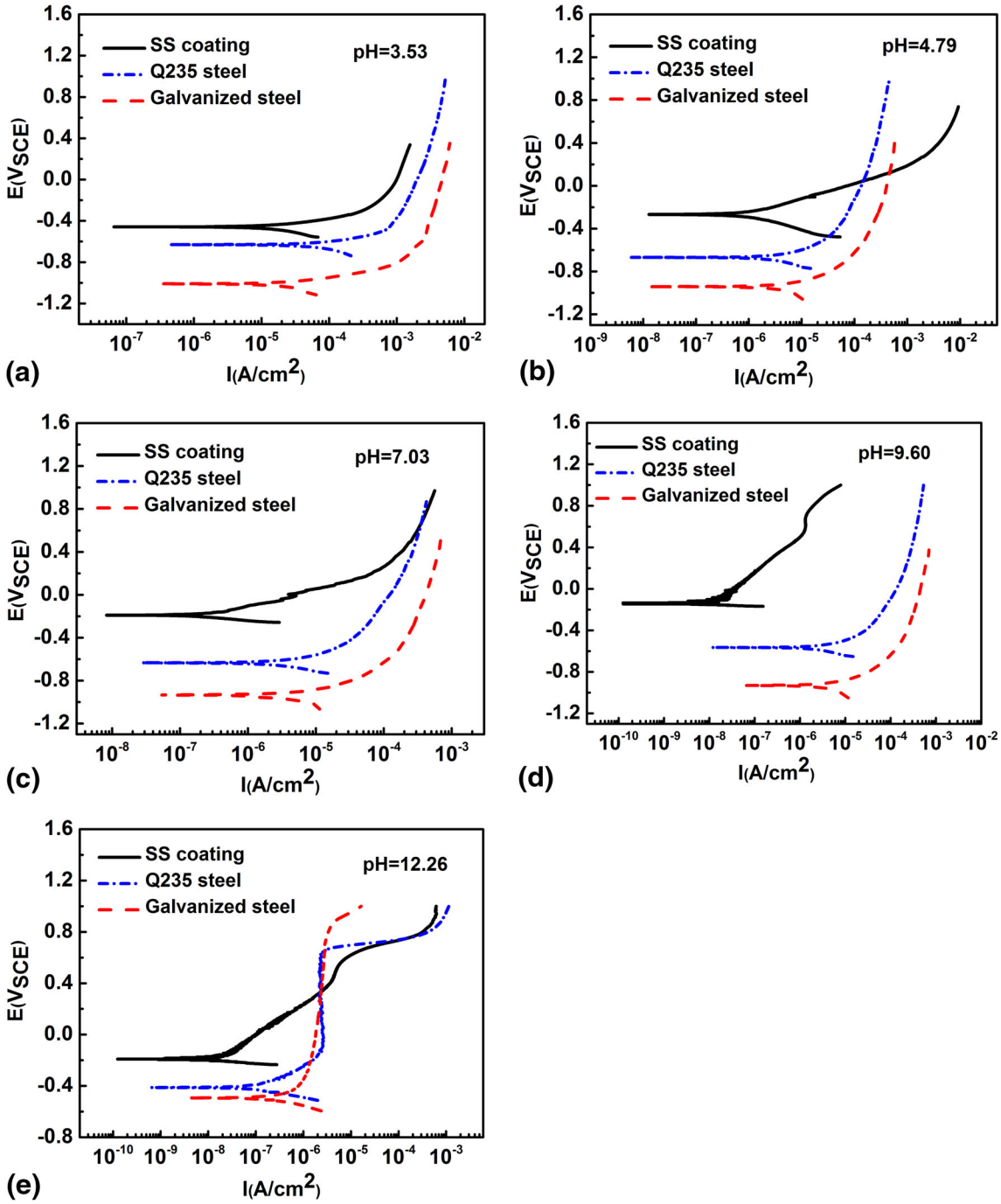

Fig. 2 Polarization curves of the three steels at different pH values

Table 3 Electrochemical parameters obtained from the Tafel extrapolation

Materials	pH value	i_{corr}, μA/cm^2	E_{corr}, mV	b_c, mV/dec	b_a, mV/dec
Q235 steel	3.53	60.73	−604.1	223.51	129.58
Galvanized steel	3.53	15.33	−1012.5	198.14	117.36
SS-coated steel	3.53	14.10	−463.9	135.70	94.80
Q235 steel	4.79	3.30	−513.1	209.02	99.04
Galvanized steel	4.79	3.16	−942.6	213.34	130.79
SS-coated steel	4.79	0.91	−271.3	126.30	141.00
Q235 steel	7.03	2.80	−502.3	167.37	108.34
Galvanized steel	7.03	2.88	−935.1	241.72	139.80
SS-coated steel	7.03	0.16	−189.7	71.46	116.94
Q235 steel	9.60	2.60	−525.3	150.64	108.24
Galvanized steel	9.60	3.50	−930.9	230.70	128.57
SS-coated steel	9.60	0.014	−220.2	37.10	101.80
Q235 steel	12.26	0.053	−416.6	69.91	96.68
Galvanized steel	12.26	0.23	−493.2	111.02	205.93
SS-coated steel	12.26	0.036	−251.1	80.80	182.40

2.2 Electrochemical Tests

The electrochemical tests were performed at room temperature and under natural aeration condition. A three-electrode cell was used with a platinum foil as counter electrode, a saturated calomel electrode (SCE) as the reference electrode with saturated KCl solution, and the test specimen as working electrode. All potentials in this study were given versus SCE. The working electrodes were sealed with epoxy resin to expose an area of 1 cm^2. The exposed faces were ground with silicon carbide papers of 2000 grit size and rinsed with de-ionized water just before the immersion.

Both linear polarization measurements and potentiodynamic polarization curves were conducted using an EG&G 273A Potentiostat. Linear polarization measurements were performed in the potential range from −20 to 20 mV_{ocp}, and the polarization resistance was fitted by PowerSuite software. The potentiodynamic polarization curves were obtained at a constant scan rate of 0.5 mV/s, and corrosion current densities (i_{corr}) were estimated by Tafel extrapolation. The detailed description about the sweep rate had been given in our previous work (Ref 13). Electrochemical impedance spectra (EIS) measurements were performed with a frequency response analyzer (EG&G 5210) coupled to a potentiostat (EG&G 273A). The frequency range was from 100 kHz to 10 mHz with an amplitude of 10 mV (rms) at open circuit potential (OCP). The obtained impedance spectra were fitted with ZSimpwin software. After each EIS measurement, potentiodynamic polarization tests were performed. Because the EIS was conducted at OCP, it would not affect the following potentiodynamic measurements too much. The potentiostatic tests were carried out only at pH 3.53 and 9.60 to further distinguish the corrosion behavior of the SS-coated steel in the solutions at different pH values. The samples for potentiostatic tests were 5 × 5 × 3 mm, which were sealed with silicone rubber except the working face. The applied polarization potential was 200 mV above the OCP, and the maintaining time was 60 min. Each experiment in this work was repeated at least three times to check the reproducibility of the measurements.

Table 1 shows the simulated soil solutions with pH value ranging from 3.53 to 12.26, based on the primary anions in soil in Yiyang area, Hunan Province, China. The electrolytes were prepared from analytical grade $MgCl{\cdot}6H_2O$, Na_2SO_4, $NaHSO_4{\cdot}H_2O$, NaOH, and de-ionized water.

2.3 Surface Analyses

X-ray photoelectron spectroscopy (XPS) analyses were carried out using an ESCALAB 250 x-ray photoelectron spectrometer. Photoelectron emission was excited by monochromatic Al Kα source operated at 150 W with initial photo energy 1486.6 eV. A survey spectrum was first recorded to identify all elements present at the surface, and then high-resolution spectra of Cr 2p, Fe 2p, Ni 2p, and C 1s were recorded. The C 1s peak from contaminative carbon at 284.6 eV was used as a reference to correct the charging shifts. The quantification of the species in the corrosion product films was performed via XPS peak 4.1 peak fitting software. The surface morphology of the specimens was examined by an INSPECT F scanning electron microscope (SEM) operating at 25 kV.

3. Results

Figure 1 shows the microstructures of the three steels used in the present work. The thickness of SS coating was about 1 mm, and the thickness of the Ni bond layer is approximately 100 μm. The SS coating displayed a wave stack lamellar structure. Small amount of holes and oxide inclusions were observed in the coating. The microstructure of Q235 steel mainly consists of pearlite and ferrite. The thickness of galvanized zinc layer is about 50 μm.

Table 2 shows the fitted polarization resistance (R_p) of the three kinds of materials at different pH values. It can be found that the R_p of as-received Q235 steel increased with increasing pH value. In strong alkaline solution, the R_p of Q235 steel increases rapidly. The corrosion behavior of galvanized steel was similar to that of Q235 steel. In acidic or near neutral solutions, the Q235 steel had smaller R_p than the galvanized steel. However, in alkaline solution, especially in strong alkaline solution, the R_p of galvanized steel was less than that of Q235 steel. It was clear that in all solutions investigated presently, the SS-coated Q235 steel exhibited the largest R_p among the three kinds of materials. The R_p of SS-coated steel increased with increasing pH value from 3.53 to 9.60, but the R_p slightly decreased with a further increase of pH value to 12.26. This indicates that the corrosion mechanism of the

coated steel in simulated soil solutions may change with increasing pH value.

Figure 2 shows the polarization curves of the three kinds of materials at different pH values. The polarization curves with no obvious Tafel region may be related to the scope of *Y*-axis (*E*) too big in the graph (from −1.4 to 1.6 V). Also, some factors can lead to the deviation of anodic polarization curves from Tafel behavior. For example, the anodic dissolution makes the surface rough, and the electrode reactions are affected by the mass transfer process due to large polarization current (Ref 14). In this case, the useful part of the curve had been enlarged to make the Tafel region more obvious, and chose the linear region or approximate linear region to carry out Tafel fitting. As the corrosion current can also be determined by cathodic Tafel curve alone, for the anodic polarization curves which exhibited passivation characteristic, the cathodic Tafel curves had been extrapolated back to zero overvoltage to determine i_{corr}. All the polarization curves were fitted on the basis of the above rules. Although there were some deviations during the fitting process, it was sufficient to estimate the corrosion resistance of materials.

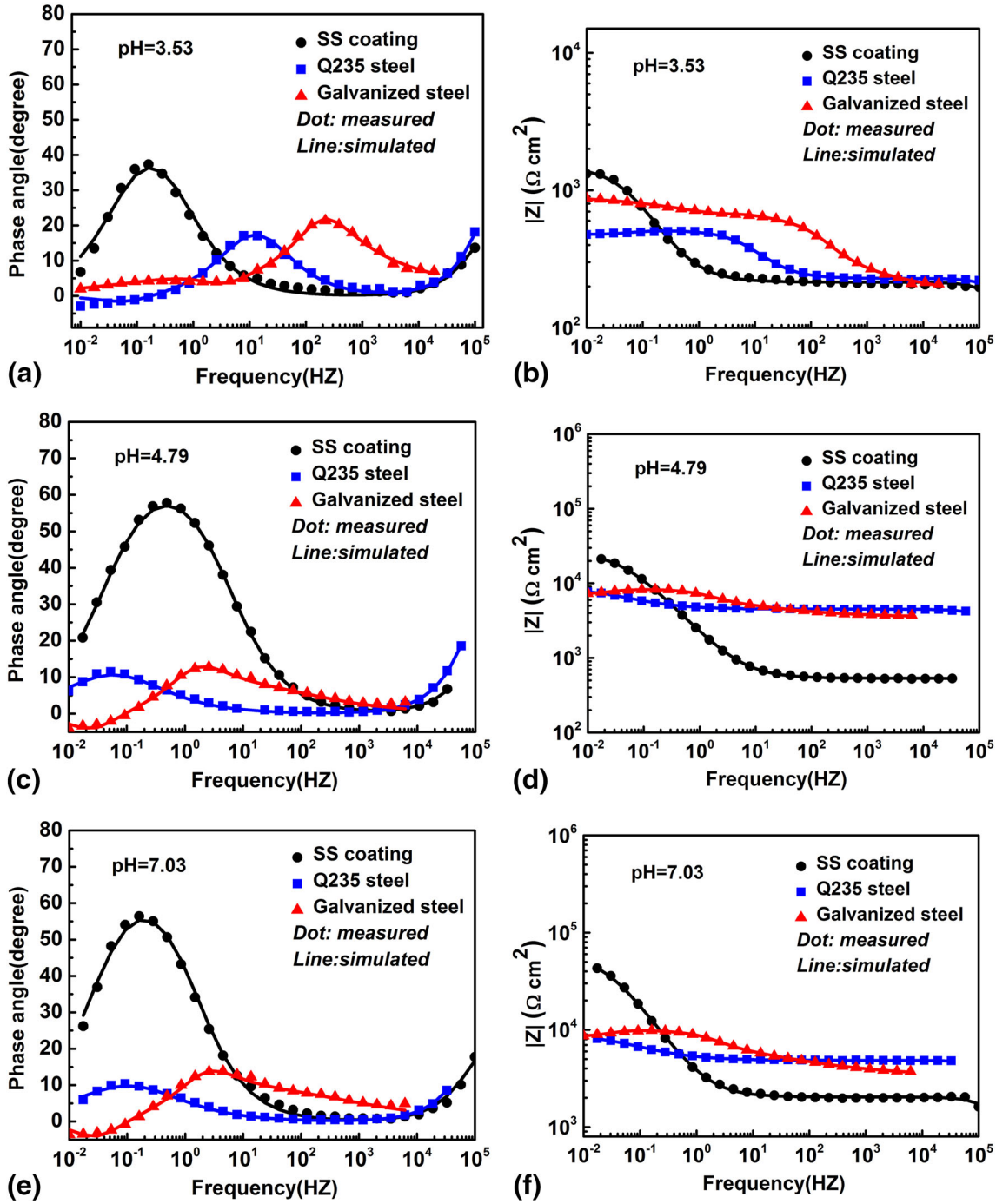

Fig. 3 Bode plots for the three steels at different pH values

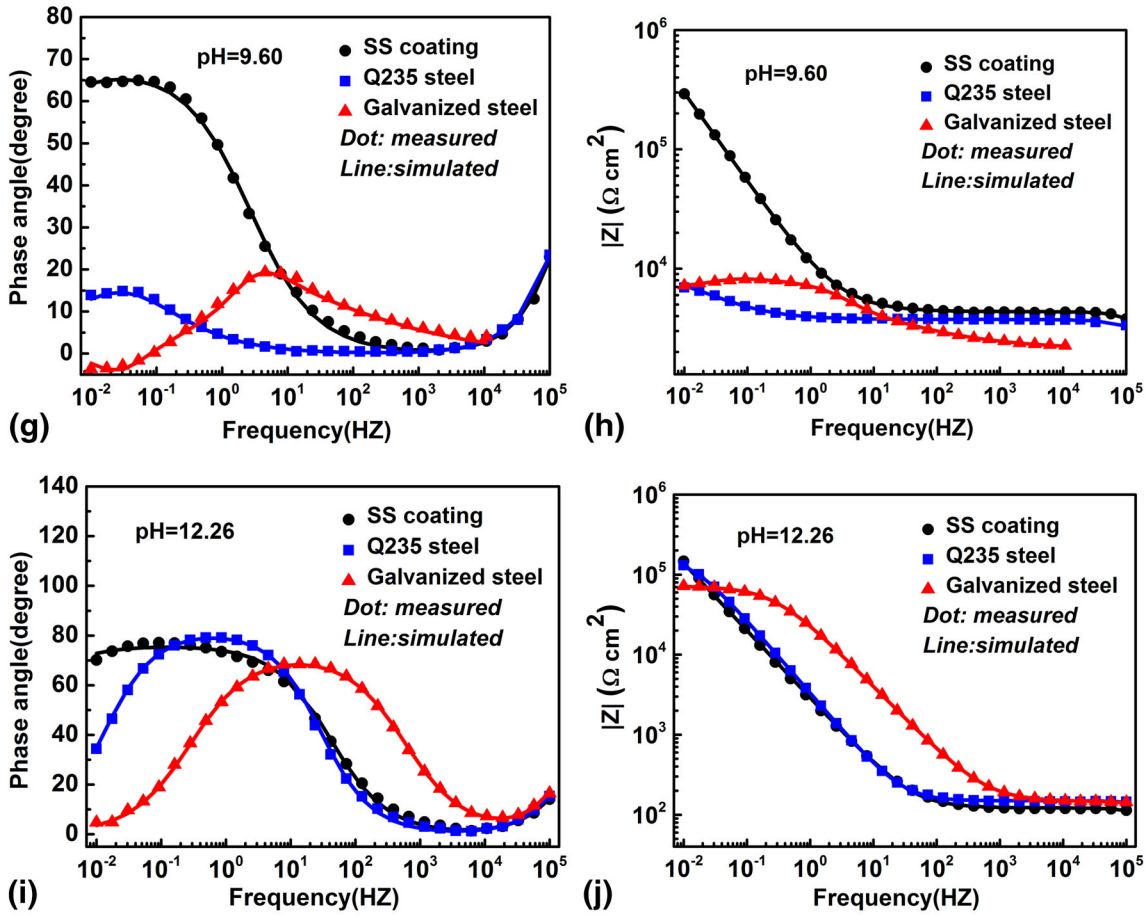

Fig. 3 continued

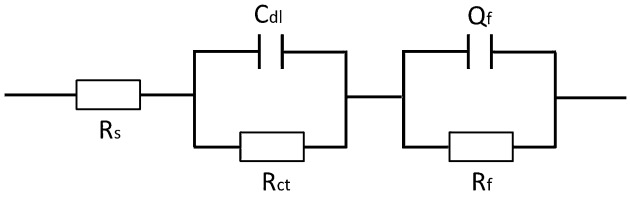

Fig. 4 Equivalent circuit used in this work

Table 3 shows the electrochemical parameters such as corrosion potential (E_{corr}), corrosion current (i_{corr}), anodic Tafel slope (b_a), and cathodic Tafel slope (b_c) obtained from the Tafel extrapolation. In all soil simulated solutions, the i_{corr} of SS-coated steel was relatively low in comparison with those of the as-received Q235 steel and galvanized steel, and the E_{corr} of SS-coated steel was more noble than those of the Q235 steel and galvanized steel. In particular in weak alkaline solution, the i_{corr} of SS-coated steel was much lower than those of the other two materials. The i_{corr} of SS-coated steel increased

Table 4 Equivalent circuit and corresponding fitted parameters

Material	pH	C_{dl}, F/cm^2	R_{ct}, Ω cm^2	Q_{film}, F/cm^2	n	R_f, Ω cm^2	L, H cm^2	R, Ω cm^2
Q235 steel	3.53	4.49×10^{-9}	148.1	1.52×10^{-4}	0.7877	2.38×10^{2}	286.70	47.14
Galvanized steel	…	5.84×10^{-6}	191.9	4.43×10^{-4}	0.3298	6.84×10^{2}	4.65	105.80
SS-coated steel	…	9.10×10^{-9}	104.9	1.89×10^{-3}	0.8011	1.30×10^{3}	…	…
Q235 steel	4.79	3.24×10^{-10}	4499	6.30×10^{-4}	0.6561	4.25×10^{3}	…	…
Galvanized steel	…	6.08×10^{-5}	1958	5.92×10^{-5}	0.4546	3.21×10^{3}	8719	1474
SS-coated steel	…	1.50×10^{-8}	58.53	2.90×10^{-4}	0.7586	1.56×10^{4}	…	…
Q235 steel	7.03	1.51×10^{-10}	4843	4.16×10^{-4}	0.63	4.38×10^{3}	…	…
Galvanized steel	…	3.70×10^{-5}	2221	4.57×10^{-5}	0.3771	5.26×10^{3}	10060	1986
SS-coated steel	…	2.50×10^{-10}	1679	4.09×10^{-5}	0.7758	4.70×10^{5}	…	…
Q235 steel	9.60	1.96×10^{-10}	2999	3.40×10^{-4}	0.6089	4.96×10^{3}	…	…
Galvanized steel	…	2.91×10^{-5}	2021	6.46×10^{-5}	0.4014	5.29×10^{3}	10640	1920
SS-coated steel	…	2.63×10^{-10}	3409	2.70×10^{-5}	0.7604	4.54×10^{6}	…	…
Q235 steel	12.26	3.01×10^{-9}	149.1	5.64×10^{-5}	0.9151	1.73×10^{5}	…	…
Galvanized steel	…	7.41×10^{-5}	16320	1.86×10^{-4}	0.6704	5.06×10^{4}	…	…
SS-coated steel	…	9.81×10^{-9}	73.5	7.39×10^{-5}	0.8443	2.58×10^{6}	…	…

continuously with the applied potential, but the higher the pH value, the slower the current density increased. When the pH value was 9.60 or so, the SS-coated steel showed the lowest i_{corr} (1.4×10^{-2} μA/cm^2), indicating that the SS-coated steel has the best corrosion resistance in weak alkaline environment. The corrosion resistance of Q235 steel and galvanized steel was in good agreement with the previous linear polarization measurement results.

Figure 3 shows the Bode plots for the three steels at different pH values. From the impedance moduli plot, at lower frequencies (around 10 mHz), the plot of SS-coated steel exhibited higher impedance values than Q235 steel and galvanized steel in each solutions, which related with the difference of polarization resistance. The impedance moduli increased as the frequency goes down. The low frequencies impedance moduli of SS-coated steel increased as the pH value increased from 3.53 to 9.60, and then decreased a little when pH value reached 12.26. The Bode phase plot shows that the phase angle peaks of SS-coated steel were much higher than Q235 steel and galvanized steel in the five solutions. With the increasing pH value, the phase angle peak of SS-coated steel increased and shifted to lower frequencies. In alkaline solution, the SS coating presented a wide phase angle peak, which may be related to the passivation.

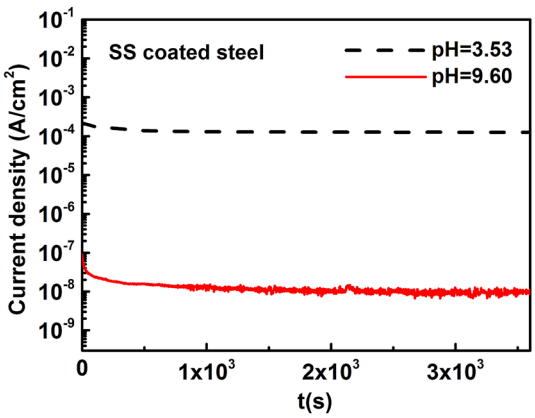

Fig. 5 Potentiostatic tests of SS-coated steel at pH 3.53 and 9.60

Figure 4 shows the equivalent circuit for EIS fitting. Elements used in Fig. 4 are as follows: R_s is the resistance of the solution; C_{dl} is the capacitance of the double layer; R_{ct} is the resistance of charge transfer which is associated with both anodic and cathodic reactions; Q_f is the constant phase element (CPE) related to the capacitance of the film, which is introduced instead of pure capacitance in simulations to obtain good agreement between the simulated and experimental data; R_f is the resistance of the film.

Because inductive features were observed in some EIS results, the equivalent circuit R_s (C_{dl} R_{ct}) (Q_f R_f) (LR) was used for these cases. According to some previous work, the inductive behavior may be related to the iron dissolution or the presence of chloride ions (Ref 15), while according to others, it could arise from adsorption and desorption of a reaction intermediate (Ref 16), but the exact reason is still unclear. The R in series with L is just used to fit the present EIS data, and its exact meaning is also unclear. However, the main aim of this work is to investigate the effects of pH value on corrosion behavior of SS-coated Q235 steel, and R_f is the most important parameter.

Table 4 shows the fitting parameters of the present experimental EIS data based on the equivalent circuit. In all simulated soil solutions, the R_f for the SS-coated steel was obviously larger than those for the as-received Q235 steel and galvanized steel, suggesting that the corrosion product film on the SS-coated steel was more protective.

Potentiostatic tests have been conducted for further understanding why the SS-coated steel exhibits different corrosion behaviors at different pH values. Two solutions have been selected, in which the SS-coated steel has the most different corrosion resistance according to the previous experimental results. After the tests, the surface morphologies and the composition of corrosion products were analyzed.

Figure 5 shows the results of potentiostatic tests at pH 3.53 and 9.60 for the SS-coated steel. Obviously, the SS-coated steel showed much lower current density in alkaline solution than in acidic solution.

Figure 6 shows the surface morphologies of the SS-coated steel after potentiostatic tests at pH 3.53 and 9.60. It was clear that the SS-coated steel suffered more serious corrosion in acidic simulated soil solution.

Figure 7 and 8 show the XPS spectra for the corrosion product scales on the SS-coated Q235 steel formed after potentiostatic tests in the solution of pH 3.53 and 9.60. At pH

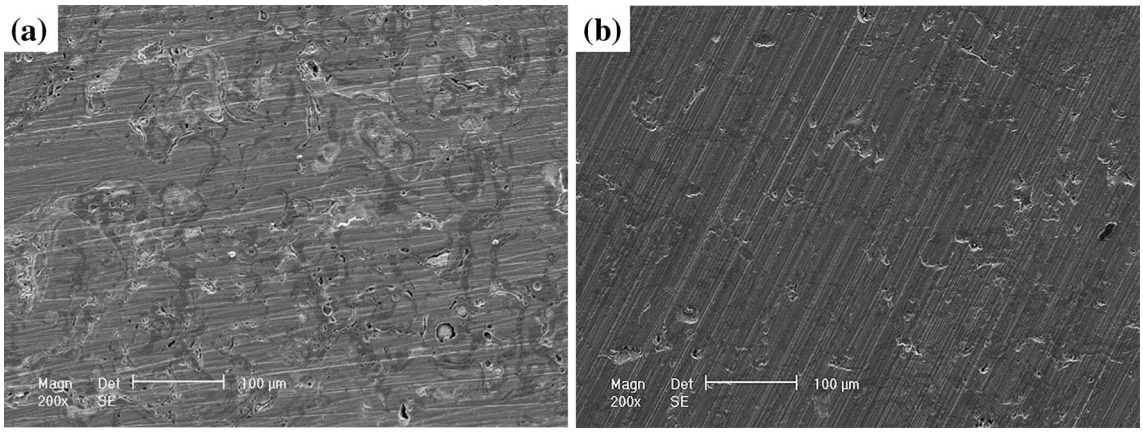

Fig. 6 Surface morphologies after potentiostatic tests of SS-coated steel at pH 3.53 (a), pH 9.60 (b)

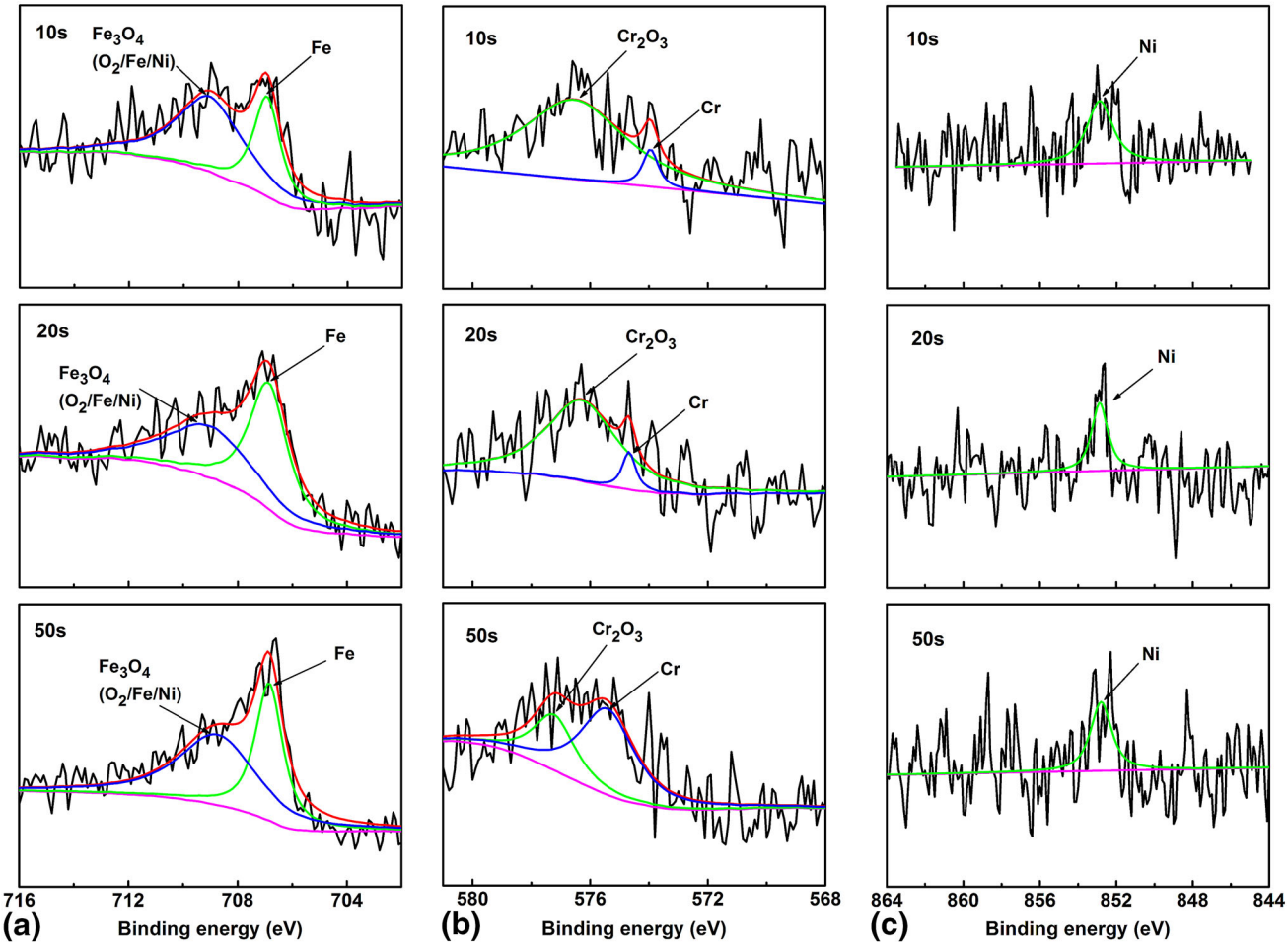

Fig. 7 Detailed XPS spectra of Fe $2p_{3/2}$, Cr $2p_{3/2}$, and Ni $2p_{3/2}$ peaks collected from corrosion product scales on the SS-coated Q235 steel formed after potentiostatic tests in the solution of pH 3.53

3.53, Fe and its oxides, Cr and its oxides were detected, while only metallic Ni^0 peaks have been detected in the corrosion product. With increasing sputtering time, the oxide peaks decreased and the metallic peaks increased. At pH 9.60, the peak around 710.9 eV was corresponding to Fe_2O_3, and the peak around 708 eV was the characteristic of Fe_3O_4 (Ref 17). There was no metallic Cr^0 peak detected at the surface while another peak around 577.3 eV emerges, which may be attributed to $Cr(OH)_2$ or Cr_2O_3 (Ref 18). On the spectra of Ni, the oxide and hydroxide peaks of Ni appeared (around 854 eV corresponding to NiO, around 856 eV to $Ni(OH)_2$ (Ref 18)) instead of the metallic Ni^0 peak in the corrosion product.

Figure 9 shows the surface morphologies of the as-received Q235 steel, galvanized steel, and thermal-sprayed SS-coated Q235 steel after 1-year field bury in Mao Jia Tang substation (Yiyang City of Hunan province in China). The soil pH value is 7.4 (water: soil is 1: 1). All the three steels have suffered from corrosion after the field bury test. The Q235 steel had the most serious corrosion with a russet rust scale formed on the specimen surface (Fig. 9a). Under high magnification, some obvious spallation was observed in the rust scale (Fig. 9b). The galvanized steel showed better corrosion resistance than the Q235 steel (Fig. 9c). But local galvanized layer on the specimen surface had been damaged, and the steel substrate was exposed (Fig. 9d). The thermal-sprayed SS-coated steel had the best corrosion resistance among the three kinds of materials. Although some rust was observed on the specimen surface (Fig. 9e), the specimen still had the original thermal-sprayed surface morphology, especially under high magnification (Fig. 9f).

4. Discussions

According to the electrochemical measurement results, the thermal-sprayed SS-coated Q235 steel has better corrosion resistance in the simulated soil solutions than the as-received Q235 steel and galvanized steel. The SS-coated steel showed the largest polarization resistance (Table 2), the lowest anodic current density (Fig. 2; Table 3), and the largest film resistance (Fig. 3; Table 4). In addition, with increasing pH value, the corrosion resistance of the SS-coated steel tended to become better, in particular in weak alkaline solution.

The polarization resistance (R_p) values were determined from the slopes of the linear polarization curves in the range of ± 10 mV about the zero current potential and are collected in Table 2. Using the Tafel slopes (b_a and b_c) which were determined by polarization curves and R_p values, the corrosion

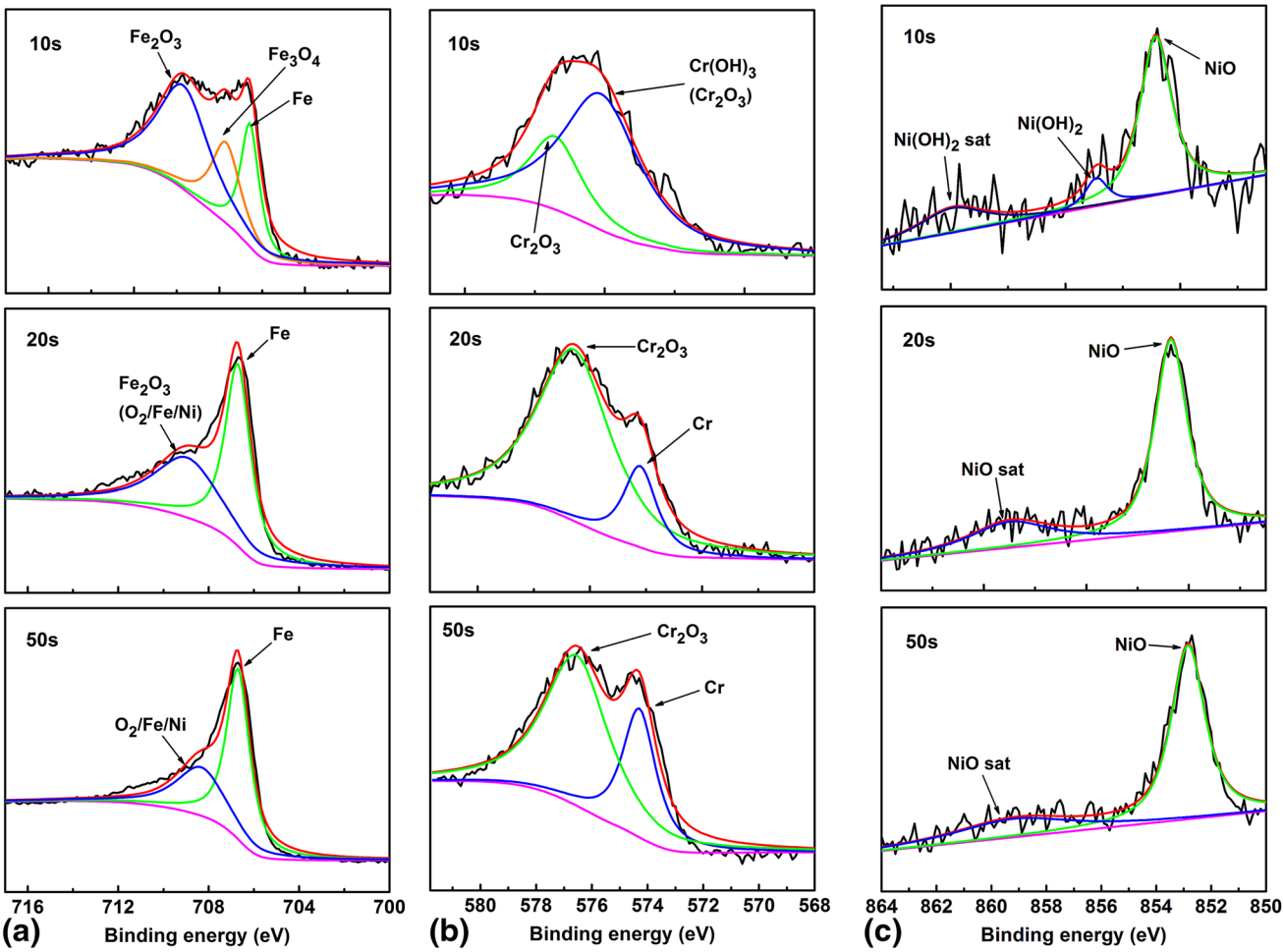

Fig. 8 Detailed XPS spectra of Fe $2p_{3/2}$, Cr $2p_{3/2}$, and Ni $2p_{3/2}$ peaks collected from corrosion product scales on the SS-coated Q235 steel formed after potentiostatic tests in the solution of pH 9.60

current density were calculated from the Stern Geary equation as follows:

$$R_p = \frac{b_a b_c}{2.303 \cdot i_{corr} \cdot (b_a + b_c)} \quad \text{(Eq 1)}$$

The results are listed in Table 5. The i_{corr} obtained from R_p showed the same change tendency as the i_{corr} determined by the Tafel extrapolation method. The i_{corr} of SS-coated steel was relatively low in comparison with those of the Q235 steel and galvanized steel. In the weak alkaline solution, the SS coating showed the lowest i_{corr} (0.037 μA/cm^2). Nevertheless, the i_{corr} obtained from R_p were bigger than the i_{corr} determined by the Tafel extrapolation method in each experiment. This may be because linear polarization resistances do not consider the existence of solution resistance.

In EIS results, R_{ct} is the resistance of charge transfer which can reflect the difficulty of electrochemical reaction. In general, the bigger the R_{ct} values, the smaller the corrosion rate, accordingly, the better the protection of the corrosion products. The charge transfer process usually reflects through the time constant of low frequency region. R_{ct} is affected by many factors, and is difficult to obtain in the present test frequency range. So, we investigated the corrosion behavior using the resistance of the corrosion production film (R_f). Also, the results were consistent with R_p and i_{corr}.

The different corrosion resistance of the SS-coated steel at pH 3.53 and pH 9.60 could be attributed to different corrosion mechanisms. In acid solution, the process of anode is mainly the active dissolution of SS coating, while in alkaline solution, the process of anode is the oxidation reaction of SS coating. According to the potential (E)-pH diagrams of M-H_2O (M = Cr, Fe and Ni) system at 25 °C (Ref 19), in strong acidic solutions, Fe tends to dissolve in the form of Fe^{2+}; Cr tends to dissolve in form of Cr^{3+}; and Ni tends to dissolve in form of Ni^{2+}, while in the weak alkaline solutions, the corresponding metal oxides are the stable corrosion products.

The present XPS results are in good agreement with the above E-pH prediction. At pH 3.53, the peaks corresponding to the metallic components are present even at the outmost surface (706.48 eV corresponding to Fe^0, 573.77 eV to Cr^0 and 852.33 eV to Ni^0) (Ref 18), especially for the spectra of Ni 2p, which indicates that the surface of SS-coated steel cannot form good protective corrosion products in strong acid solution. At pH 9.60, Cr_2O_3/$Cr(OH)_3$, NiO, $Ni(OH)_2$, Fe_2O_3, Fe_3O_4, and metallic Fe^0 are detected at the beginning of the sputtering. As

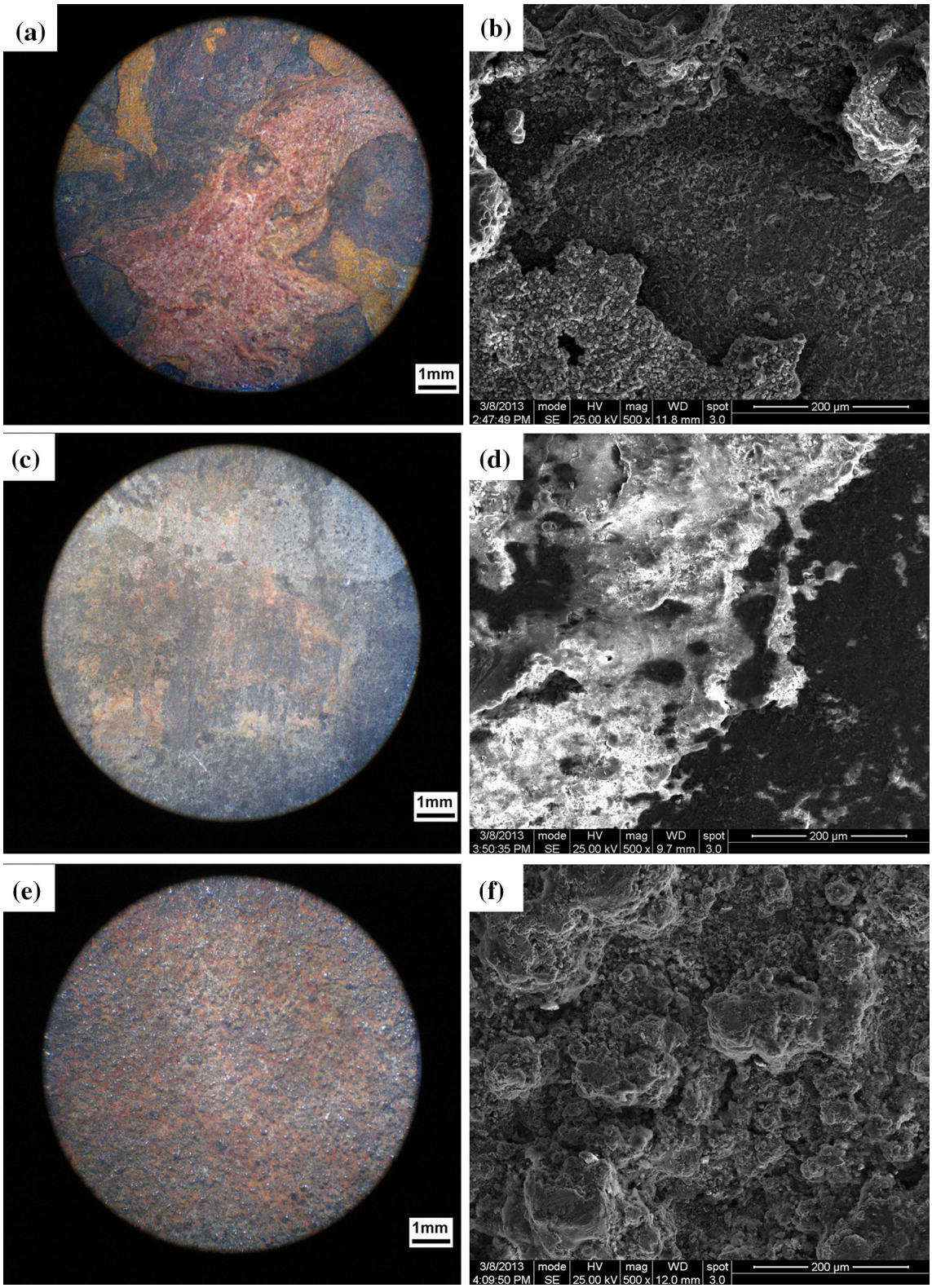

Fig. 9 Surface morphologies of the as-received Q235 steel, galvanized steel, and thermal-sprayed SS-coated Q235 steel after 1-year field bury test: (a, b) the as-received Q235 steel; (c, d) galvanized steel; (e, f) SS-coated Q235 steel

proposed by Sun et al (Ref 20), the OH^- was associated with Cr dominantly to form the Cr^{3+} hydroxide at the alloy/solution interface due to lower standard free energy of $Cr(OH)_3$ than Cr_2O_3. The OH^- could diffuse inward through the oxide film and react with the Cr from the alloy at the metal/film interface according to reaction (2) (Ref 21).

Table 5 Corrosion current densities i_{corr} (μA/cm^2) obtained from polarization resistances

pH values	3.53	4.79	7.03	9.60	12.26
Q235 steel	73.74	4.44	3.10	2.96	0.097
Galvanized steel	32.96	4.11	3.54	4.21	0.37
SS-coated steel	16.82	1.90	0.154	0.037	0.081

$$2Cr + 6OH^- = 2Cr(OH)_3 + 6e^- \quad \text{(Eq 2)}$$

Then, the $Cr(OH)_3$ can be changed into Cr_2O_3 according to reaction (3) (Ref 22):

$$Cr(OH)_3 + Cr = Cr_2O_3 + 3H^+ + 3e^- \quad \text{(Eq 3)}$$

It is believed that the surface of SS-coated steel will gradually form dense and protective oxide film if the time of corrosion in weak alkaline solution is extended. But when pH value increases to 12.26, the excess OH^- will lead to the dissolution of the corrosion product scales according to the reactions (4) and (5), which degrades the corrosion resistance of the SS-coated steel. As a result, the SS-coated steel showed the best corrosion resistance in weak alkaline solutions.

$$Cr(OH)_3 + OH^- = CrO_2^- + 2H_2O \quad \text{(Eq 4)}$$

$$Cr_2O_3 + 2OH^- = 2CrO_2^- + H_2O \quad \text{(Eq 5)}$$

The field bury tests further proved that the thermal-sprayed SS-coated Q235 steel has better anti-corrosion performance than the as-received Q235 steel and galvanized steel, suggesting that such kind of coating may be of great perspective to improve the service life of grounding mesh.

5. Conclusions

Electrochemical corrosion behaviors of the as-received Q235 steel, galvanized steel, and thermal-sprayed SS-coated Q235 steel have been investigated in simulated soil solutions in the present work. Some conclusions could be drawn as follows:

1. The electrochemical tests prove that the thermal-sprayed SS-coated Q235 steel has the best corrosion resistance among the three kinds of materials. With increasing pH value from 3.53 to 12.26, the corrosion resistance of the SS-coated Q235 steel becomes better. In weak alkaline solutions, the SS-coated Q235 steel shows the largest polarization resistance (3.2×10^5 Ω cm^2), the lowest anodic current density (1.4×10^{-2} μA/cm^2), and the largest film resistance (4.5×10^6 Ω cm^2).
2. The pH-dependent corrosion resistance of the thermal-sprayed SS-coated Q235 steel is due to the different corrosion mechanisms and corrosion product scales. In acid solution, the surface of the SS-coated steel cannot form good protective corrosion product scales, while in alkaline solution the corrosion product scales consist of metal oxide (Fe_2O_3, Fe_3O_4, Cr_2O_3, and NiO) and hydroxide ($Cr(OH)_3$, $Ni(OH)_2$).
3. The 1-year field bury tests prove that the thermal-sprayed SS-coated Q235 steel has the best corrosion resistance among the above three kinds of materials, suggesting that such kind of coating may be of great perspective to improve the service life of grounding mesh.

Acknowledgments

This work was jointly supported by the Science Project of State Grid Corporation of China under Grant KG12K16004, the Science and Technology Project of Yunnan Province, the Technology Development (Cooperation) Fund from Yunnan Wenshan Dounan Manganese Industry Co., Ltd., and the Innovation Fund of Institute of Metal Research (IMR), Chinese Academy of Sciences (CAS).

References

1. Y.F. Yu, Y.Z. Zhan, Z.W. Lin, and Z. Yuan, Research on 220 kV Substation Ground Grid Corrosion Status in Hubei Power Grid, *Hubei Electr. Power*, 2007, **31**, p 5–7
2. A.J. Yan, X. Chen, and L.J. Feng, Soil Corrosion Performance of Several Grounding Net Materials, *Corros. Sci. Prot. Technol.*, 2010, **22**, p 197–199
3. F.J. Yan and X.G. Li, Corrosion and Protection of Grounding Net in Electric Power System, *Shandong Electr. Power Technol.*, 2007, **34**, p 15–18
4. ANSI/IEEE Standard No. 80-2000, *IEEE Guide for Safety in AC Substation Grounding*, The Institute of Electrical and Electronics Engineers, New York, 2000
5. M.C. Zheng, Z.N. Chen, and J.H. Li, Research on Corrosion Characteristics of Corrosion Rule and Anti-corrosion Technology of Grounding Device for Large Substations, *East China Electr. Power*, 2009, **37**, p 1463–1467
6. M. Loboda and R. Marciniak, Field Corrosion Test in Poland of Copper Coated Steel Earthing Rods for LPS, *29th International Conference on Lightning Protection*, Sweden, 2008, p 5–9
7. Y.H. Wu, T.M. Liu, C. Sun, J. Xu, and C.K. Yu, Corrosion Behaviors of Copper in Acidic Soil Acidified with Simulated Acid Rain, *J. Sichuan Univ.*, 2010, **42**, p 119–125
8. J.S. Chen, Copper Grounding Conductor Cause Harm. http://www.500kv.net/copper.html
9. Anonymous, Thermal Spray Coatings Protect Steel Structures from Corrosion, *Adv. Mater. Process.*, 2007, **165**, p 114–115
10. S. Papavinsasam, M. Attard, B. Arseneult, and R.W. Revie, State-of-the-Art of Thermal Spray Coatings for Corrosion Protection, *Corros. Rev.*, 2008, **26**, p 105–146
11. Z. Zeng, N. Sakoda, and T. Tajiri, Corrosion Behavior of Wire-Arc-Sprayed Stainless Steel Coating on Mild Steel, *J. Therm. Spray Technol.*, 2006, **15**, p 431–437
12. H.T. Cai, T. Jiang, and Y. Zhou, Research Status and Development of the Thermal Spray Technology, *Equip. Manuf. Technol.*, 2014, **42**, p 28–32
13. X.Q. Wu, J. Xu, W. Ke, S. Xu, B. Feng, and B.T. Hu, Effects of pH Value on Corrosion Behavior of Thermal-Sprayed Al-Si Coated Q235 Steel in Simulated Soil Solutions, *J. Mater. Eng. Perform.*, 2014, **23**, p 2265–2273
14. C.N. Cao, *Principles of Electrochemistry of Corrosion*, Chemical Industry Press, Beijing, 2008
15. M. Keddam, O.R. Mattos, and H. Takenouti, Mechanism of Anodic Dissolution of Iron-chromium Alloys Investigated by Electrode

Impedances—I. Experimental Results and Reaction Model, *Electrochem. Acta*, 1986, **31**, p 1147–1158

16. R.F.A. Jargenlius-Pettersson and B.G. Pound, Examination of the Role of Molybdenum in Passivation of Stainless Steels Using AC Impedance Spectroscopy, *J. Electrochem. Soc.*, 1998, **145**, p 1462–1469
17. H. Sun, X.Q. Wu, and E.H. Han, Effects of Temperature on the Properties of the Oxide Film Formed on 304 SS in High Temperature Lithium Borate Buffer Solution, *Corros. Sci.*, 2009, **51**, p 2840–2847
18. J. Xu, X.Q. Wu, and E.H. Han, The Evolution of Electrochemical Behaviour and Oxide Film Properties of 304 Stainless Steel in High Temperature Aqueous Environment, *Electrochim. Acta*, 2012, **71**, p 219–226
19. H. Sun, "Electrochemical Corrosion Behaviors and Oxide Film Properties of Stainless Steels and Nickel-Based Alloys in High Temperature and High Pressure Aqueous Environments", Ph.D. Thesis, Chinese Academy of Sciences, 2010
20. H. Sun, X.Q. Wu, and E.H. Han, Effects of Temperature on the Protective Property, Structure and Composition of the Oxide Film on Alloy 625, *Corros. Sci.*, 2009, **51**, p 2565–2572
21. A. Machet, A. Galtayries, S. Zanna, L. Klein, V. Maurice, P. Jolivet, M. Foucault, P. Combrade, P. Scott, and P. Marcus, XPS and STM Study of the Growth and Structure of Passive Films in High Temperature Water on a Nickel-Base Alloy, *Electrochim. Acta*, 2004, **49**, p 3957–3964
22. S.E. Ziemniak, M.E. Jones, and K.E.S. Combs, Solubility and Phase Behavior of Cr(III) Oxides in Alkaline Media at Elevated Temperatures, *J. Solut. Chem.*, 1998, **27**, p 33–66